


Article

The Relationship between the Time Difference of Formation Water Infiltration Rate, Tectonic Movement, and the Formation Pressure Coefficient

Xiaoping Mao ¹, Shuxian Li ^{1,*}, Xiurong Chen ², Xuehui Li ¹, Fan Yang ¹, Yuexing Yang ¹ and Zhen Li ¹

¹ School of Energy Resources, China University of Geosciences, Beijing 100083, China; maosp9@163.com (X.M.); 18810629073@163.com (Z.L.)

² Department of Computer Science and Technology, Tsinghua University, Beijing 100084, China; chenxiurong@mail.tsinghua.edu.cn

* Correspondence: 16608941103@163.com

Abstract: The study of formation pressure holds great significance for both exploration and development. The formation pressure coefficient is a crucial parameter in geology, encompassing various aspects. Numerous models exist to explore its influencing factors, yet they remain highly controversial. Our research has gathered data on formation pressure states and tectonic movement rates from dozens of large sedimentary basins worldwide. We delved into the patterns of formation pressure changes during basin deposition, subsidence, and tectonic uplift, taking into account the permeability of formation water. The findings reveal that during the Neogene and beyond, rapid deposition or tectonic uplift can cause the infiltration of formation water to lag behind tectonic movements, resulting in overpressure. Conversely, if recent tectonic movements are slow, formation water will complete its infiltration process ahead of tectonic changes, bringing the formation pressure to a hydrostatic state. Consequently, we have concluded that abnormal formation pressure primarily depends on the rate of tectonic movements during the Neogene and Quaternary periods. This study also proposes four formation pressure models, paving the way for a comprehensive understanding of formation pressure within a unified theoretical framework.

Keywords: tectonic movement; overpressure; pressure compartment; hydrocarbon generation and pressurization; sedimentary process



Citation: Mao, X.; Li, S.; Chen, X.; Li, X.; Yang, F.; Yang, Y.; Li, Z. The Relationship between the Time Difference of Formation Water Infiltration Rate, Tectonic Movement, and the Formation Pressure Coefficient. *Appl. Sci.* **2024**, *14*, 5615. <https://doi.org/10.3390/app14135615>

Academic Editor: Dibyendu Sarkar

Received: 8 May 2024

Revised: 14 June 2024

Accepted: 19 June 2024

Published: 27 June 2024



Copyright: © 2024 by the authors. Licensee MDPI, Basel, Switzerland. This article is an open access article distributed under the terms and conditions of the Creative Commons Attribution (CC BY) license (<https://creativecommons.org/licenses/by/4.0/>).

1. Introduction

Stratigraphic pressure is an extremely important physical quantity in geological research, with overpressure and ultrahigh pressure receiving particular attention. This phenomenon is observed in approximately two-thirds of sedimentary basins worldwide [1] and in over half of China's hydrocarbon-producing layers [2]. Given its close association with hydrocarbon distribution, overpressure has become a pivotal aspect of research in hydrocarbon accumulation dynamics [3–7]. In China, formation pressure is commonly classified as ultra-low pressure (pressure coefficient <0.75), low pressure (0.75–0.9), normal pressure (0.9–1.2), high pressure (1.2–1.5), and ultra-high pressure (>1.5) [8]. The effect of overpressure on oil and gas is multifaceted. It not only influences the hydrocarbon generation process of organic matter and the occurrence state of hydrocarbons but also concerns the dynamics and direction of migration. In addition, overpressure plays a significant role in the preservation and destruction of gas reservoirs and has a profound impact on the spatial distribution of oil and gas reservoirs, such as episodic hydrocarbon expulsion [9], episodic charging and episodic reservoir formation [10], and overpressure migration [11]. Moreover, overpressure can contribute to high hydrocarbon production [12]. Meissner (1987) [13] proposed a pressure cycle controlled by hydrocarbon generation, transitioning from initial normal hydrostatic pressure to abnormal high pressure (due to

hydrocarbon generation and expansion), then to abnormal low pressure (as migration halts and hydrocarbon dissipation exceeds supply), and finally back to normal pressure. Additionally, overpressure implications extend to the safety of drilling and geological engineering operations and the development planning of oil and gas fields [14,15]. Therefore, the distribution and genesis mechanism of overpressure have always been of great concern to geologists and exploration workers, and the significance of research in this area is profound.

The causes of overpressure have been widely discussed, with undercompaction, hydrocarbon generation, and tectonic compression being recognized as the three common pressure-increasing mechanisms [16–20]. Wang et al. (2019) [21] proposed that tectonic compression can reduce porosity, thereby generating overpressure. The two most common causes of abnormally high pressure in petroleum basins are compaction disequilibrium and hydrocarbon generation [22]. Osborn and Swarbrick (1997) [23] suggested that unbalanced compaction is a viable mechanism for overpressure during rapid burial of thick mudstone sequences while dismissing other mechanisms, sparking significant debate. Bethke (1986) [24] quantitatively analyzed the efficiency of dehydration during the transformation of smectite to illite on formation pressure, concluding that its effect is negligible. Both undercompaction and hydrocarbon generation are considered the primary factors leading to overpressure. Qiu et al. (2020) [25] argued that most factors causing abnormal pressure occur only under specific conditions, with undercompaction, hydrocarbon generation, and tectonic stress remaining the most common controlling factors. Due to the influence of overpressure genesis, there can be a negative effect on the generation of hydrocarbons. For instance, the overall impact of overpressure on the thermal evolution of organic matter can be divided into four levels, but generally, it has an inhibitory effect, albeit with varying degrees of inhibition [26].

In summary, there are various factors that can cause formation overpressure. Currently, there is no single mechanism that can explain overpressure under all conditions. For example, undercompaction can only explain overpressure during the sedimentation process but not during uplift. Tectonic compression can explain overpressure in foreland basins but cannot explain overpressure in extensional fault basins. Hydrocarbon generation and pressurization can cause overpressure, but they cannot explain overpressure in the absence of oil and gas. For example, the Kela 2 gas field has overpressure, but Kela 1 and Kela 3, which do not contain oil and gas, still exhibit ultra-high pressure. Each hypothesis can only explain a specific type of overpressure, indicating that these piecemeal, customized, or patchwork theories of overpressure genesis may inherently have some flaws. Generally speaking, the more geological factors listed, the further away we may be from the truth. Whether there is a unified, truly dominant factor that can explain formation pressure under different conditions is the goal of this article to explore in depth.

A common, yet often overlooked factor, is formation water, which plays a pivotal role in underground geological fluids. It is a crucial element throughout the entire process from the initial development of sedimentary basins to the advanced diagenesis stage and should be considered the dominant force. However, most scholars believe that the osmotic effect of formation water on formation pressure is less efficient in pressure increase compared to other factors, leading to a general disregard for its impact [27]. Neuzil (1995) [28] demonstrated unbalanced abnormal pressure phenomena from the perspective of formation water dynamics, controlled by compaction (with a high deposition rate of >200 m/Ma), diagenesis, and deformation, independent of hydrocarbon generation. Nevertheless, this has not garnered sufficient attention. Indeed, due to the small radius of water molecules, groundwater in most lithologic formations transitions relatively quickly from an abnormal pressure state to a more balanced hydrostatic pressure state compared to the timescale of tectonic movements. However, in well-sealed mudstones, shales, and gypsum–salt layers, there is a certain lag in water infiltration when formation pressure changes, and equilibrium is not achieved instantaneously or within a short period relative to tectonic movements. Therefore, exploring the nature of formation overpressure from the perspective of formation water is of great significance, as it may help us uncover the truth.

This article focuses on the changes of formation water before and after diagenesis and attempts to explore the relationship between abnormal pressure variations and formation water. By combining the permeability of formation water, four models of formation pressure evolution are proposed, and an analysis of major basins both domestically and internationally reveals their universality. It is also suggested that formation water has been fully discharged through the seepage process before diagenesis, eliminating the possibility of undercompaction due to inadequate drainage. After diagenesis, formation water completes the transition from overpressure to normal pressure through permeation, and this switch does not result in a significant increase in porosity.

2. Data and Methodology

The data utilized in this study comprises basin formation pressure states, tectonic evolution histories, and tectonic movement rates from over 50 basins or regions both domestically and internationally. Additionally, measured data on organic and inorganic pores from 163 overpressured strata in 11 basins or regions were included, along with calculations of their respective proportions.

The method of study is to analyze the pressure changes of stratigraphic water in the formation of sedimentary basins and the process of diagenetic evolution. In porous media, the water is smaller than other hydrocarbon molecules, and 3.2 \AA ($1 \text{ \AA} = 10^{-10} \text{ m}$), so there is water penetration in places with abnormal stress. The following Table 1 shows the effective diameter of different molecules [29]. Under the conditions of formation, the deeper the pressure, the local if there is a condition that exceeds the hydrostatic force condition, the water has the tendency to permeate and tend to the hydrostatic pressure.

Table 1. Effective of different molecules (Unit: \AA).

Molecule	Effective Diameter \AA	Molecule	Effective Diameter \AA
H ₂ O	3.2	C ₃ H ₈	5.1
He	2.0	Benzene	4.7
CO ₂	3.3	Normal alkanes	width: 4.2 length: 4.2~4.8
N ₂	3.4	Cyclohexane	5.4
CH ₄	3.8	Complex cyclic compounds	15~20
C ₂ H ₆	4.4	Bitumen	>50

Although water has strong permeability, there is a certain lag time in strata of different lithologies, and the process is not instantaneously completed. According to the Poiseuille formula [30,31], assuming a mudstone stratum thickness of 200 m and a pore radius of 2 nm, it only takes 1.5 Ma for the formation water in the reservoir to drop from an initial 2.6 times overpressure to 1.2 times overpressure due to the permeability of the mudstone, as shown in Table 2. Wu (2024) [32] studied the pore size distribution of 7 shale samples from the Shahejie Formation in the Jiyang Depression and found that pores ranging from 0–4 nm accounted for 59%, indicating that this pore radius is reasonable. During rapid accumulation, the initial condition is that both the stratum and stratum framework bear the crustal stress together, so 2.6 is taken. This calculation can at least illustrate that the permeability of water in the stratum is relatively fast.

During the syngenetic and early diagenetic stages, due to higher porosity and permeability coefficients, the formation pressure remains at hydrostatic pressure (normal pressure). The subsequent analysis in this article mainly focuses on strata in the middle and late diagenetic stages.

Table 2. Timetable for overpressure relief of mudstone with different pore sizes and thicknesses.

Pore Size (nm)	Thickness (m)					
	50	100	200	500	1000	2000
Pressure relief to 1.6 times:						
1	0.297	1.189	4.756	29.723	-	-
2	0.074	0.297	1.06	7.43	29.723	-
5	0.012	0.048	0.190	1.189	4.756	19.023
10	0.003	0.012	0.048	0.297	1.189	4.756
20	0.001	0.003	0.012	0.074	0.297	1.189
50	0	0	0.002	0.012	0.048	0.190
Pressure relief to 1.2 times:						
1	0.376	1.506	6.022	37.640	-	-
2	0.094	0.376	1.506	9.410	37.640	-
5	0.015	0.060	0.241	1.506	6.022	24.090
10	0.004	0.015	0.06	0.376	1.506	6.022
20	0.001	0.004	0.015	0.094	0.376	1.506
50	0	0	0.002	0.015	0.06	0.241

A set of regional cap rocks with certain sealing properties may contain multiple lithologies, such as thick shale, gypsum–salt rock, and thin sand layers. To maintain overpressure in the formation itself or its underlying sandstone reservoir, it is necessary to calculate the time required for pressure relief. The calculation can be approximated by the following formula:

$$t = A \sum_{i=1}^n \frac{S_s h_i^2}{K_i} \quad (1)$$

In the formula, t represents the required time (s), h_i is the thickness of each sublayer (m), and K_i is the permeability coefficient of each sublayer (m/s). The S_s represents the water storability (1/m). A represents the dissipation coefficient, which can be taken as 1.5. Moreover, n represents the number of layers.

According to Li et al. (2024), the S_s can be taken as 0.0008 [33]. Based on the research by Yu et al. (2008) [34], the permeability coefficient of mudstone caprock can be taken as 4×10^{-12} m/s. Calculating separately for caprock thicknesses of 100 m, 200 m, 300 m, and 500 m, the required time for abnormal pressure release in the strata is approximately 0.23 Ma, 0.9 Ma, 2.1 Ma, and 5.71 Ma. These calculations are indicative and show that the process of formation water permeation is not instantaneous but relatively fast compared to geological timescales.

3. Two Modes of Forming Overpressure

Based on the characteristics of formation water and its relationship with the rate of tectonic movement, two potential modes for the formation of overpressure have been proposed. The first mode involves rapid subsidence leading to overpressure, as exemplified by the Nanpu Sag. The second mode is associated with rapid tectonic uplift, leading to overpressure, as observed in the Sichuan Basin.

3.1. Active Overpressuring (Overpressure Formed by Rapid Subsidence)

Statistics show that overpressure is prone to occur in strata at the mesodiagenetic and telodiagenetic stages when there is rapid deposition and subsidence in the basin during recent geological periods, such as the Neogene, especially the Quaternary. The following three conditions need to be met: (1) The strata where overpressure occurs require a higher degree of diagenesis, ranging from the mesodiagenetic to the telodiagenetic stage. (2) The rapid subsidence should have occurred relatively recently, during the Neogene or Quaternary; more distant rapid subsidence, such as in the Paleogene or earlier strata,

cannot form overpressure. (3) The current depth of deposition and burial exceeds the maximum burial depth in its geological history. At this time, compaction, cementation, and other diagenetic processes are still continuing, pores are decreasing, pore water is pressurized, and there is not enough time for pressure relief. The strata are still in the process of deposition and subsidence, leading to the formation of overpressure. This process is called active pressurization, or rapid subsidence overpressure, i.e., deposition and subsidence occur faster than the permeation rate of formation water.

The widespread existence of overpressure in the Shahejie Formation of the Nanpu Sag, with a maximum overpressure of up to 1.6 times the normal pressure [35], is shown in Figure 1. Weak overpressure is observed in the second and third members of the Dongying Formation, while overpressure occurs in the first member of the Shahejie Formation. The second and third members of the Shahejie Formation exhibit abnormally high pressure. The pressure distribution within the formation does not completely align with the formation trend and can cross different geological times and layers.

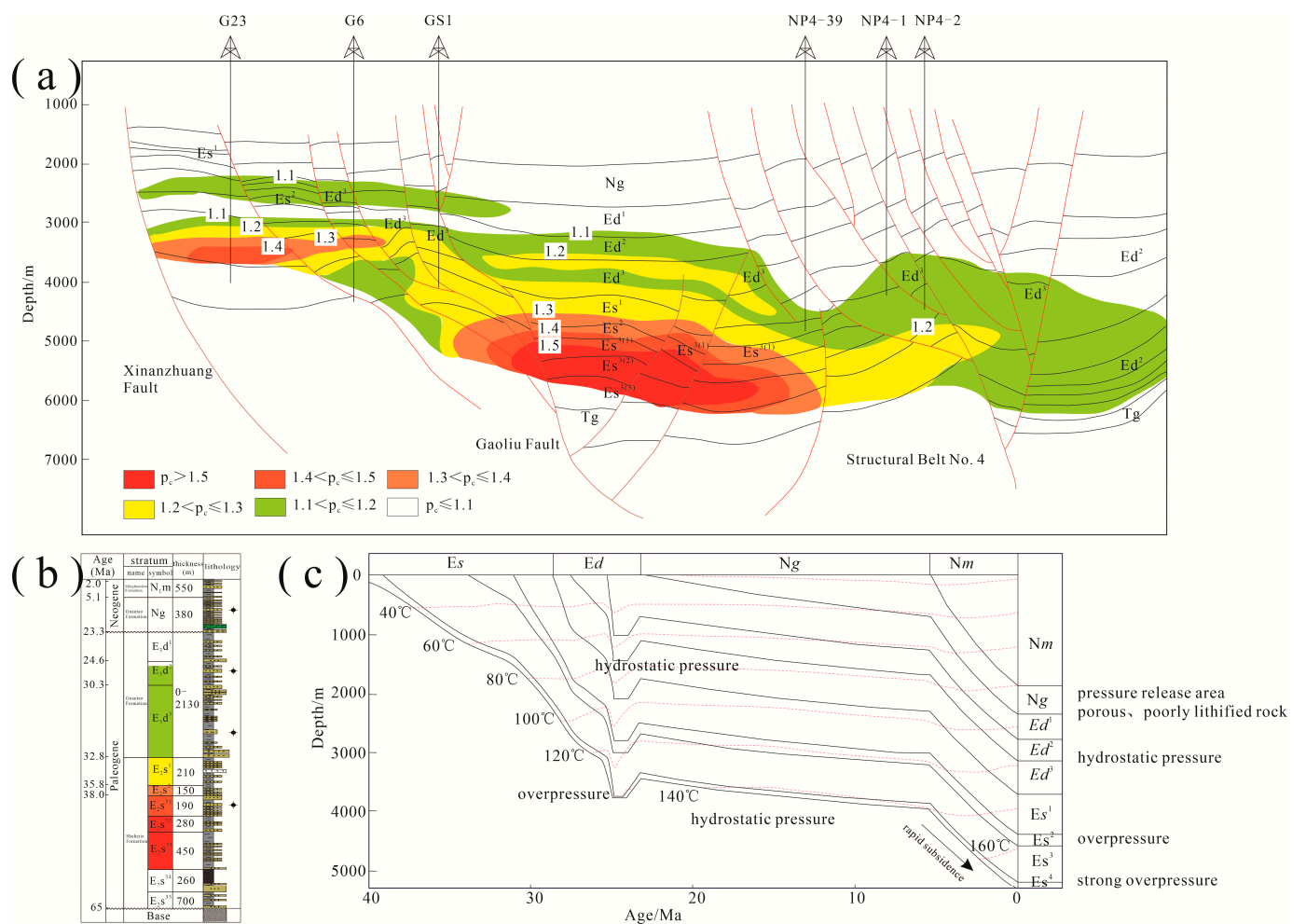


Figure 1. Reservoir pressure profile and sedimentary burial history characteristics of Nanpu Sag. (a) Profile of formation pressure in the eastern part of Nanpu sag (NNW-SSE direction); (b) Comprehensive stratigraphic column; (c) Sedimentation and burial history.

The following is an explanation of the reasons for overpressure in the Nanpu Sag using the high permeability of formation water as an example. Recently, two sets of strata have been rapidly deposited. One is the Late Miocene Guantao Formation with a maximum thickness of 1 km, and the other is the Pliocene Minghuazhen Formation with a thickness of 2 km. This has resulted in a time lag between the permeation of formation water and the speed of tectonic movement. In the late rifting stage of the Nanpu Sag,

towards the end of the Dongying Formation deposition, faulting activities ceased, resulting in a relatively long period of tectonic stability. During this time, the third member of the Shahejie Formation (Sha-3) was buried at a depth of 3 km, and the formation pressure was hydrostatic, allowing for the completion of the permeation process of formation water. Subsequently, during the depression period, the 1-kilometer-thick Guantao Formation was deposited at a relatively rapid rate, deepening the Sha-3 to a depth of 4 km. The Shahejie Formation had largely completed mechanical compaction and entered the early stage of the middle diagenesis phase A1 [36]. During this stage, pores continued to shrink, and the increase in overburden load led to a situation where both the fluid and the rock matrix shared the total overburden pressure.

To describe this process, we borrow the idea from McKenzie's (1978) instantaneous tensile model [37]. We decompose the sedimentary process into an instantaneous deposition to more concisely analyze the stabilization of its temperature and pressure fields. As shown in Figure 1, it is assumed that at the end of the Dongying Formation deposition, the third member of Shahejie Formation is at a depth of 3 km, which is in the transition period of fault depression. At this time, the formation pressure is a hydrostatic pressure of 30 MPa. Afterwards, 1 km of the late Miocene Guantao Formation was deposited, and the load of the overlying strata will be applied to the pore fluid and skeleton of the third member of Shahejie Formation. The initial formation pressure is calculated as $30 + 25$ MPa. However, the overpressure borne by the pores will decay with time, changing to $30 + 10$ MPa. During the deposition of the Minghuazhen Formation, due to the short time period, it can be qualitatively assumed that its formation pressure will remain at 80% (represented by a , where $a = 0.8$). Therefore, the formation pressure at this time is $30 + [10 + (25 - 10) \times 0.8] = 52$ MPa.

Subsequently, during the Pliocene, the Minghuazhen Formation with a thickness of 2 km was deposited, adding another 2×25 MPa of overlying pressure. This pressure also acts on the pore fluid. Since the Minghuazhen Formation dates back approximately 2.1 million years, which is a relatively short period of time, the pore water pressure has not had time to dissipate. Therefore, the final formation pressure is calculated as $52 + 50 = 102$ MPa. At this point, the depth is 6 km, and when converted into a pressure coefficient c , it is 1.67, which is basically consistent with actual measurements. Although the Dongying Formation developed lacustrine mudstone, due to the long exposure time of its top surface and the development of coarse-grained sedimentary facies such as braided rivers and meandering rivers in the Neogene Guantao and Minghuazhen Formations, its formation pressure can quickly permeate and form normal pressure. However, the abnormally high-pressure formation water in the Shahejie Formation needs to pass through the thick mudstone layer of the Dongying Formation to completely relieve pressure (permeate). Therefore, in the short term, the Shahejie Formation can still maintain abnormally high pressure. That is, the thicker the covering layer and the better the sealing layer, the longer the time to maintain abnormal pressure, resulting in a higher pressure coefficient as one goes deeper (Figure 1).

According to the aforementioned condition (2), during earlier periods such as the Paleozoic and Mesozoic, even if there was rapid deposition and subsidence at a certain stage, high formation pressure would be relieved due to the long duration of time.

In summary, the time difference between the permeation of formation water and tectonic movement can provide a good semi-quantitative explanation for the evolution of formation pressure.

3.2. Passive Pressurization (Overpressure Formed by Rapid Tectonic Uplift)

For strata in the mesodiagenetic and telodiagenetic stages, overpressure can also form after recent rapid tectonic uplift, known as passive pressurization (or passive overpressure). This is because strata with higher diagenesis have poor permeability, and pore fluid pressure will be maintained for a period of time after uplift. The cementation process surrounds the fluid and slows down the pressure release process. Although the uplift process may

cause some pressure loss due to pore rebound and cooling, it is an order of magnitude smaller compared to the new pressure coefficient c converted at a shallower depth. Passive pressurization also needs to follow the aforementioned conditions (1) and (2).

The mainstream view of most scholars currently is that uplift should result in a low-pressure trend. Their main argument is that after uplift, temperature decreases, pressure drops, and rebounding increases pores, leading to an increase in the available space for fluid volume within the pores. According to the formula of state for liquid water, formation pressure would then decrease [38]. However, these viewpoints do not adequately consider the permeation process of formation water. Both the Wufeng–Longmaxi shale formation and the Triassic Xujiahe formation in the Sichuan Basin commonly exhibit high overpressure, as shown in Figure 2. Essentially, this is the result of recent (Pliocene) rapid tectonic uplift exceeding the rate of water permeation process completion. Similar to the aforementioned active overpressure, the closer the tectonic uplift occurred to the present day, the better, especially during the Neogene and Quaternary periods.

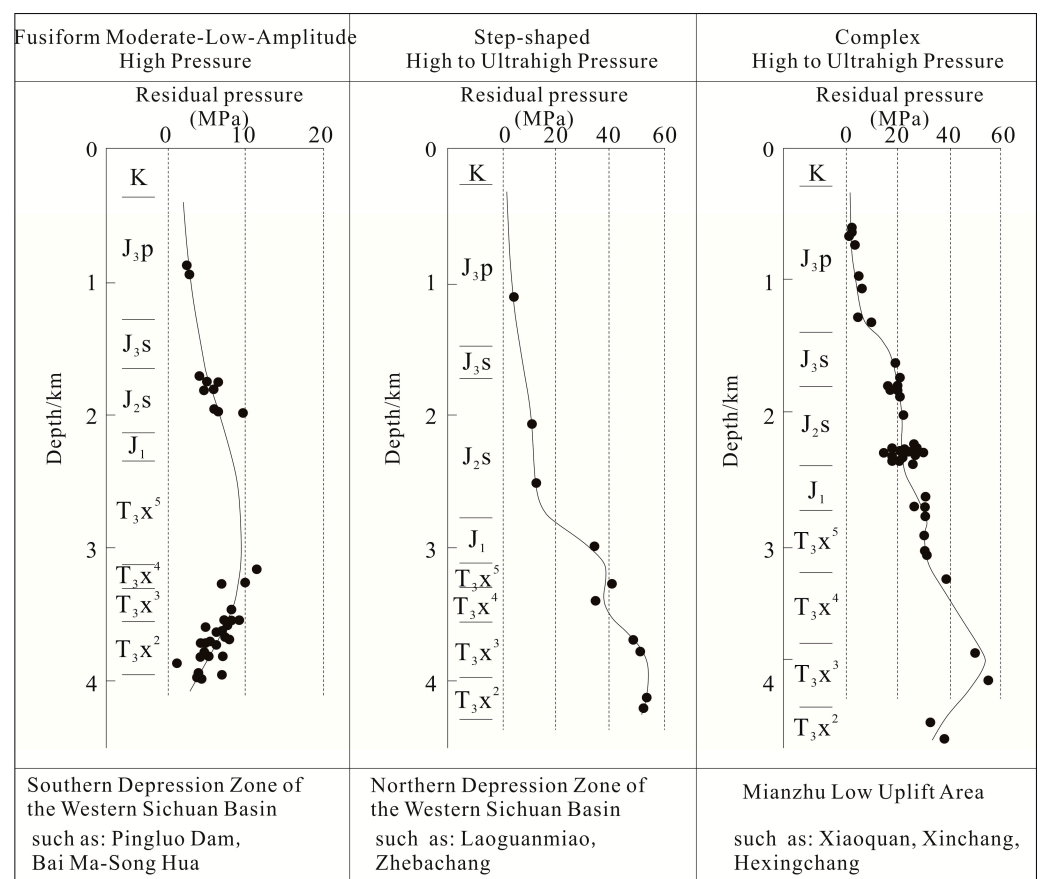


Figure 2. Distribution of residual pressure in current formations in the western Sichuan region [21].

According to Deng et al. (2009) [39], their research on the restoration of surface denudation in the Sichuan Basin reveals that the basin experienced two intense uplifts during the Cenozoic Era. Specifically, the Paleogene uplift averaged approximately 4000 m, while the Neogene uplift was about 3000 m. The target layer, the Xujiahe Formation of the Upper Triassic, currently has a burial depth of approximately 4 km. Assuming an initial state at the end of the Cretaceous, where the formation was under normal pressure with a burial depth of 11 km and an initial formation pressure of 110 MPa. This formation pressure is assumed to be the result of long-term permeation of pore water, forming a normal hydrostatic pressure due to decompression, independent of the effective stress on the framework. After the Paleogene uplift of 4 km, the depth decreased to 7 km. If this process had occurred over a prolonged period, the pressure would have

theoretically dropped to a hydrostatic pressure of 70 MPa due to decompression. However, water permeation has a certain lag and would not have completely reduced to hydrostatic pressure. Additionally, the reduction in overlying strata weight only serves to “decompress” the formation matrix. The effective stress (supporting stress) experienced by the formation matrix (framework) should be significantly higher than 110 MPa. Assuming a matrix density of 2.6 g/cm^3 , the effective stress on the matrix would be approximately 286 MPa (calculated as $11 \text{ km} \times 26 \text{ MPa/km} = 286 \text{ MPa}$). Moreover, the overpressured stratum has already lithified. Temporarily disregarding factors such as uplift rebound of stratum thickness, pore enlargement, and pressure reduction due to cooling (their magnitudes will be estimated in later chapters), the pore pressure remains essentially unchanged. A reduction in the weight of the overlying stratum can only decrease the skeletal support stress, while the pressure within the pores can still be maintained at 110 MPa. Only through a prolonged period of pressure relief can it slowly decrease to the normal hydrostatic pressure of 70 MPa, corresponding to a depth of 7 km. At the end of the Paleogene, this pressure coefficient had already increased to 1.57 due to uplift.

As evolution progressed to the Neogene period, pressure attenuation needs to be considered. At this point, based on the length of burial time, similar to what was mentioned earlier, a qualitative formation pressure retention coefficient $a = 0.8$ is assigned. This reduces the pressure coefficient from 110 MPa to 88 MPa. During the Neogene period, there was a further uplift of 3 km, changing the depth from 7 km to 4 km. Similarly, due to the relatively short time since then, it can be considered as having no attenuation. Therefore, after two uplifts and based on the new depth of 4 km, the pressure coefficient c increases to 2.2. Studies by multiple scholars have indicated that the uplift during the Neogene period occurred relatively recently, likely during the Late Cenozoic era. Electron spin resonance dating has determined that the oldest age of the Dayi conglomerate in the western Sichuan Basin is between 2.6 and 3.6 Ma. Many regions along the northern edge of the Tibetan Plateau have also deposited a similar set of coarse-grained sediments, such as the Xiyu conglomerate and Jishi conglomerate, with paleomagnetic and fission track ages dating back to the Late Cenozoic (2.5 to 3.5 Ma). This reflects that the latest period of intense uplift in the Tibetan Plateau and Sichuan Basin ended around 2.5 Ma [40]. Compared to other geological timescales, this period is relatively short, and the pore fluid pressure has not had sufficient time to dissipate. Figure 3 shows the burial history of the Sichuan Basin, indicating that the era of the latest rapid uplift and denudation is relatively recent.

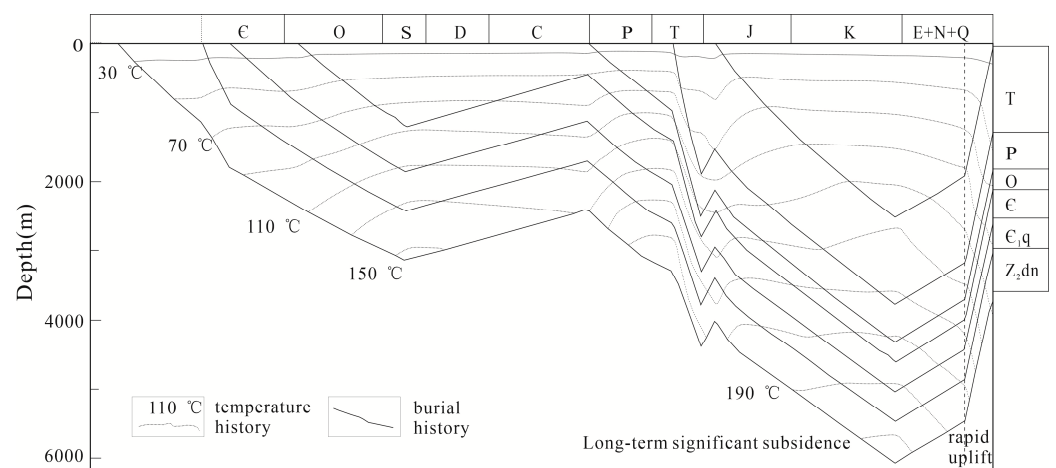


Figure 3. Comprehensive analysis of the causes of abnormal pressure in the Dengying Formation (Z2d) of the well W117 in the Sichuan Basin [25].

If it is a recent rapid uplift, the following approximate formula can be used to calculate the uplift and denudation thickness Δh :

$$\Delta h = p \times 100 - z_{pmax} \quad (2)$$

where p represents the formation pressure at the depth z_{pmax} , which corresponds to the maximum formation pressure coefficient, measured in MPa. Using this value for calculations is more accurate as other well sections, such as shallower depth intervals, may rapidly decompress during uplift and become distorted. This formula is only an approximation, as it may involve multiple recent episodes of uplift.

This model requires that the faster the uplift speed and the closer the time of uplift to the present, the better. The closely spaced JY1, PY1, and LY1 wells (<50 km) in the Wulong area on the southeastern edge of the Sichuan Basin all began to uplift during the Cretaceous period. However, JY1 experienced rapid uplift in a relatively recent time, resulting in a 1.5-fold passive overpressure in the Wufeng–Longmaxi shale formation. In contrast, PY1 and LY1 underwent uniform and slow uplift, leading to normal or low pressure, fully validating this reasoning. Most shale oil and gas basins in the United States are characterized by normal to low pressure, which is typically associated with long-term slow uplift and denudation processes that began a considerable time ago. For example, the New Albany shale in the eastern part of the Illinois Basin has been undergoing tectonic uplift since the early Triassic period with a pressure coefficient of 0.98. The Antrim shale in the Michigan Basin has experienced prolonged uplift following the deposition of Jurassic strata, resulting in a pressure coefficient of 0.4–0.6. The Barnett shale formation in Eastland County, Fort Worth Basin, has been uplifting since the end of the Cretaceous period K1 with a pressure coefficient of 1.0. Relatively speaking, the tectonic uplift of the Eagle Ford shale formation in South Texas occurred more recently, starting with rapid uplift at 15 Ma during the Miocene, resulting in a pressure coefficient of 1.27 and weak overpressure, forming a phenomenon of rapid uplift and passive overpressure.

At present, there is no unified understanding of the causes of overpressure. Relatively recognized causes include hydrocarbon generation and pressure boosting, tectonic compression, hydrothermal pressure boosting, undercompaction, pore rebound, and temperature reduction after uplift. These mentioned phenomena may all exist, but compared to the recent tectonic changes proposed in this paper, the impact on formation pressure is 1–2 orders of magnitude smaller.

4. Formation of Normal or Low Pressure Patterns

4.1. Normal Pressure Pattern

When tectonic movement is slower than the permeation rate of formation water, normal pressure will occur, referred to here as the long-term static normal pressure pattern. Due to slow tectonic uplift, subsidence, or stagnant tectonic activity, formation water has sufficient time to leak, resulting in normal pressure.

Since the beginning of the Cenozoic era, the Songliao Basin has maintained a tectonically stable (dormant) static phase for an extended period, in a state of normal to slightly elevated pressure [41].

The tectonic activity in the Erlian Basin stagnated during the Late Cretaceous and maintained a very slow uplift for 100 Ma (Figure 4). As a result, the Late Cretaceous strata exposed on the surface did not consolidate into rock and remained in a long-term static dormant state, as shown in the figure below (modified from Chen et al. (2015)) [42]. Xu et al. (2007), in explaining the normal pressure in the Erlian Basin, used analogies with the Yinggehai Basin and the Bohai Bay Basin. They employed the classic anomaly of a sudden increase in mudstone porosity at depths of 1500–2500 m to argue that the absence of a high-porosity zone in this depth range in the Erlian Basin indicates the absence of overpressure [43]. However, they overlooked the fact that many areas in the second member of the Tengger Formation in the Erlian Basin have been eroded by nearly 1000–2000 m [44],

and there is artificiality in the porosity fitting of the Yinggehai Basin. Thus, the use of undercompaction to explain the cause of overpressure is clearly unsuccessful.

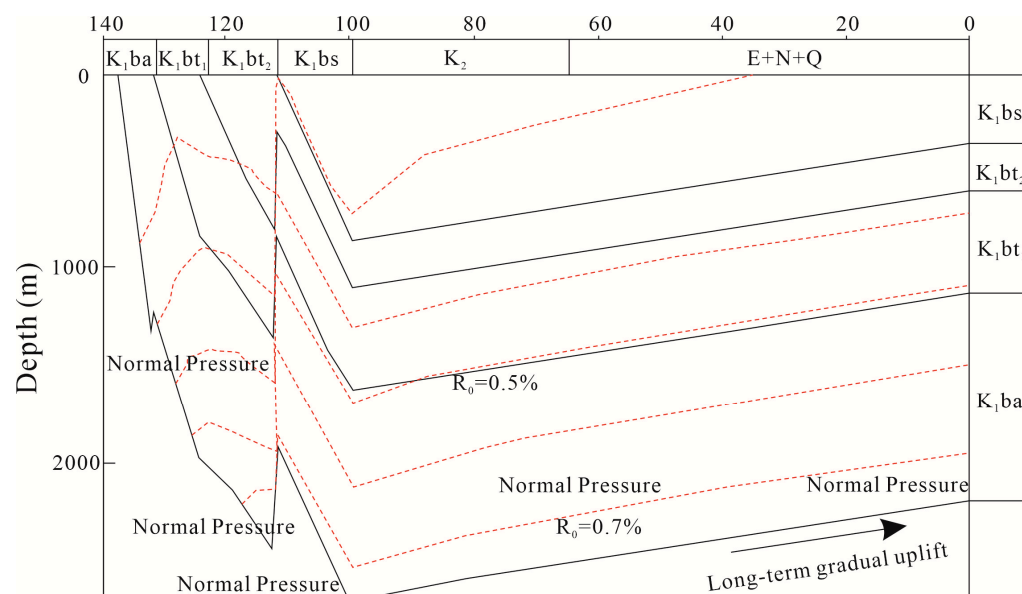


Figure 4. Burial history of well Ba 5 in the Erlian Basin, the red dotted lines in the figure show temperatures history [42].

4.2. Large Uplift and Small Subsidence Low Pressure Pattern

Large uplift and small subsidence refer to a long-term significant uplift followed by a rapid but small-scale subsidence that does not reach the maximum burial depth in history. Taking the Sulige gas field as an example, it is an abnormally low-pressure gas field. Since the Late Cretaceous (about 95 Ma), it has been in a state of uplift and denudation for an extended period, with a relatively slow denudation rate, allowing sufficient time for the internal overpressure to release. Another possible reason is that the Mesozoic strata in the northern Ordos region have relatively coarse lithology, with no development of source rocks and poor capping layers [45]. The sealing ability of the overlying strata is poor, and the mudstone layers have thinner individual and cumulative thicknesses, leading to rapid water permeation and pressure relief, resulting in low pressure.

A more important reason may be that the ancient uplifted terrain was higher than it is now. According to the research by Zhao et al. (2009), the Weihe, Yinchuan, and Hetao fault depressions formed successively at the end of the Paleocene to Eocene, and their timing and tectonic patterns are no different from those of the Bohai Bay and other basins in the east. The Shanxi Graben System developed later [46]. Li et al. (2012) concluded that the Sulige gas field experienced a small-scale sedimentary subsidence during the Neogene [47]. This means that since the Cenozoic era, there have been fluctuations rather than continuous uplift, resulting in a possible uplift to a higher elevation than present after the Late Cretaceous, followed by a long period of static conditions. After releasing pressure, hydrostatic pressure (normal pressure) was formed, as shown in Figure 5. The shallowest top surface of the P₂s in the Shihezi Formation is 3120 m; during the Neogene, there was a small-scale subsidence, and the P₂s lowered to 3210 m, not having enough time to adjust by “replenishing water” to the dense He 8 reservoir section and not yet returning to normal hydrostatic pressure, forming the present abnormally low-pressure gas reservoir. In the aforementioned active overpressure model, when a new sedimentary load is added to the original equilibrium state, there is a tendency for pore space to shrink, allowing fluids within the pores to share the load of the overlying strata. However, this does not occur during small-scale subsidence after uplift. Because the latest subsidence did not reach the maximum depth in history (the P₂s lowered to 4150 m at the end of the Early Cretaceous, 97 Ma), the organic matter maturity and porosity would remain at their maximum states,

and the diagenesis process would stagnate. The fluids within the pores would not share the additional overlying load with the skeleton until the latest subsidence exceeds the original maximum depth, at which point compaction and increased maturity and other diagenesis processes would resume. Therefore, the numerical deviation of abnormal low pressure from normal pressure can be used to qualitatively calculate the relative height of the highest uplift during geological history compared to the present. The formula is as follows:

$$\Delta h = 100(P_j - P) = 100(z_j/100 - P) = z_j(1 - c) \quad (3)$$

where Δh represents the uplift height in meters (m), P represents the formation pressure at the measuring point in megapascals (MPa), P_j represents the hydrostatic pressure at the corresponding depth z_j of the measuring point in megapascals (MPa), z_j represents the depth of the measuring point in meters (m), and c represents the pressure coefficient.

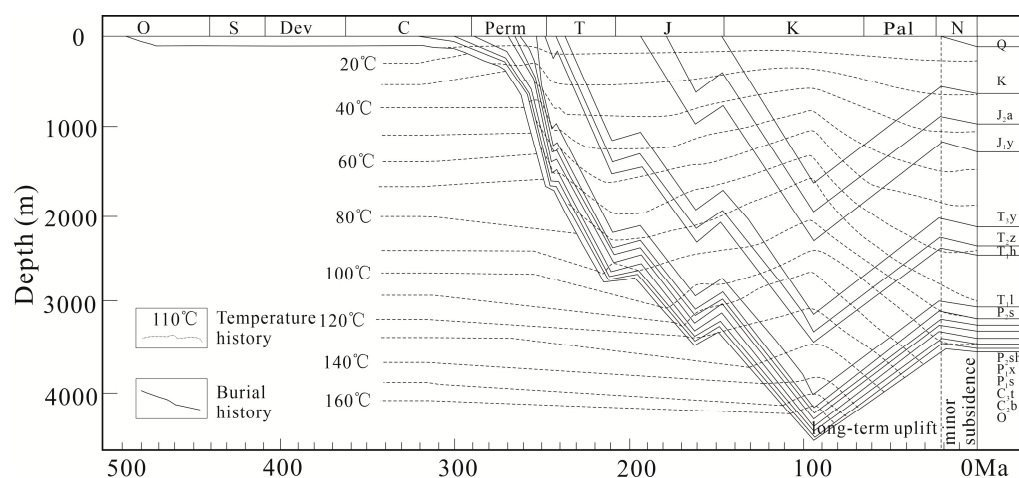


Figure 5. Burial history, thermal evolution history, and inclusion trapping time of well Su 16 in the Sulige gas field [47].

The pressure coefficient of the Sulige gas reservoir is relatively low (with an average of 0.85), and the main layer has a deep burial depth (with an average of 4000 m). Based on these calculations, its uplift height is approximately 600 m higher than it is now.

In summary, the formation of overpressure may be influenced by factors such as hydrocarbon generation, aquathermal pressurization, and undercompaction, but these factors are not determinative. Instead, overpressure is primarily caused when the rates of uplift and subsidence exceed the permeation rate of formation water. The impact of overpressure on hydrocarbon reservoirs should also be adjusted accordingly. For instance, overpressured compartments can facilitate the accumulation of hydrocarbons, promote hydrocarbon expulsion, episodic hydrocarbon expulsion, episodic charging, and episodic accumulation. These processes can be summarized into the following four models (Table 2 and Figure 6):

- (1) The active overpressure model of rapid subsidence is known as the Nanpu Model, as shown in Figure 6a.
- (2) The passive overpressure model of rapid tectonic uplift is known as the Sichuan Model, as shown in Figure 6c.
- (3) The long-term static normal pressure model is known as the Songliao Model, as shown in Figure 6b.
- (4) The model of significant uplift followed by minor subsidence and low pressure is known as the Sulige Model (low pressure), as shown in Figure 6d.

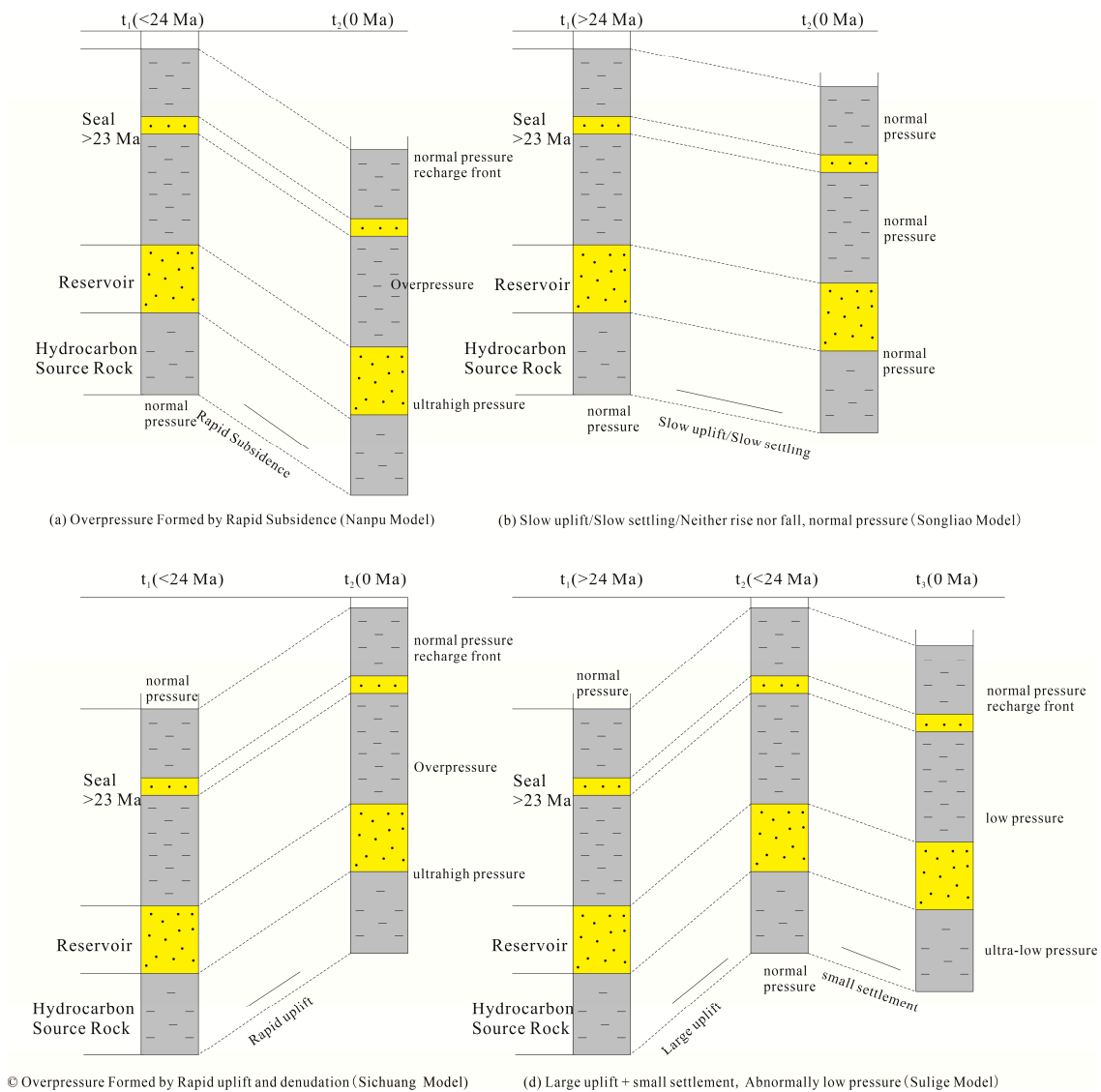


Figure 6. Four models of formation pressure.

These four models can determine the formation pressure state within a unified theoretical framework, eliminating the need to adopt different hypotheses for formation pressure in different situations (tension, compression, uplift, subsidence, and with or without oil and gas involvement) (Table 3).

Table 3. Four models of formation pressure conditions.

Number	Models	Factor	Characteristics of Tectonic Movement	Pressure State	Examples
1	Nanpu Model	Active overpressure	Rapid subsidence	Overpressure	Nanpu Oilfield Qaidam Basin Sichuan Basin
2	Sichuan Model	Passive overpressure	Rapid uplift and denudation	Overpressure	Kuqa Depression Junggar Basin
3	Songliao Model	Long-term static	Slow uplift Slow settling Neither rise nor fall	Normal pressure	Songliao Basin Erlian Basin Baise Basin
4	Sulige Model	Large uplift and small subsidence	Large uplift + small settlement	Abnormally low pressure	Sulige Gas Field

5. Verification of Universality

To demonstrate the validity of the aforementioned argument, this paper also examines the formation pressure characteristics of multiple basins or regions both domestically and internationally. It is found that formation pressure is entirely dependent on the pattern and rate of Cenozoic tectonic movements.

5.1. Example of Active Rapid Overpressure

The Kuqa Depression is a depression with ultra-high pressure, with a maximum pressure coefficient of 2.2. There are numerous research papers on its genesis, mainly suggesting that the intense tectonic compression during the late Himalayan period is the primary factor contributing to the formation of abnormal high pressure in the Kuqa Depression [48,49]. In fact, this region experiences active pressurization. The deposition of an extremely thick gypsum salt layer in the Miocene Jidike Formation (N_{1j}) slows down the permeation of formation water, followed by the deposition of the Kangcun Formation (N_{1K}) with a thickness ranging from 200 to 1300 m. Most importantly, the Pliocene Kuqa Formation (N_{2K}) with a thickness of 450 to 3600 m and the Quaternary Q with a maximum thickness of 1000 m were deposited only 5.2 Ma. Both Dina 202 and Tuzi 2 in the eastern Kuqa Depression are subject to tectonic compression. The former experienced rapid deposition of $N_{1K} + N_{2K}$ greater than 3 km, resulting in a pressure coefficient of 2.2, while the latter experienced deposition greater than 1 km, leading to a pressure coefficient of only 1.8 [50]. The pressure coefficient is controlled by the thickness of rapid deposition. This is a typical case of active overpressure.

An abnormal high pressure was observed at approximately 3300 m in the third member of the Shahejie Formation (E_{s3}) in the Maxi trough, located in the northeastern part of the Raoyang sag in the Jizhong depression. The maximum pressure coefficient reached 1.37 [51]. Similar to the aforementioned Nanpu Sag, the combined thickness of the Guantao Formation, Minghuazhen Formation, and Pingyuan Formation in this region exceeds 2000 m, indicating active overpressure resulting from recent rapid sedimentation and subsidence.

If there is continuous rapid deposition combined with multiple well-sealed gypsum salt layers, the pressure coefficient will be even higher. In the Shizigou area of western Qaidam Basin, there is continuous rapid deposition and subsidence with a total thickness of 2530 m, consisting of 730 m in the Miocene, 1200 m in the Pliocene, and 300 m in the Quaternary Qigequan Formation. At well S23, which is located in the center of gypsum salt deposition, multiple gypsum salt layers are developed, with a single layer thickness of up to 164 m and a cumulative thickness of 325 m. The maximum pressure coefficient in the lower Ganchaigou Formation E_3 (buried depth of about 3800 m) is 2.0, indicating ultra-high pressure [52].

The main source rocks in the Yinggehai-Qiongdongnan Basin are the Oligocene Yacheng Formation and the Miocene Meishan and Sanya Formations, making it the basin with the strongest overpressure among the Cenozoic basins in eastern China and offshore areas. Overpressure is commonly developed below 2800–3000 m, and the measured pressure coefficient (the ratio of formation pressure to hydrostatic pressure) in some intervals is higher than 2.0 [53]. The fundamental reason is the rapid accumulation of sediment during the Quaternary, with a maximum thickness of nearly 2512 m and an extremely high deposition rate.

5.2. Example of Long-Term Static Low Pressure

The Alberta Basin in Canada is a well-studied basin characterized by abnormally low pressure [54–56]. The Mississippian to Cretaceous hydrostratigraphic sequence in the southwest region of the basin can be divided into the following two major systems: (1) the lower system consisting of the Mannille Group from the Mississippian to the Lower Cretaceous, and (2) the upper system consisting of the Colorado Group in the upper part of the Lower Cretaceous to the Edmonton Group at the top of the Upper Cretaceous. Since

the end of the Cretaceous, the basin has been in a long-term static state, which is consistent with the long-term static low-pressure model.

The main sedimentary strata in the Baise Basin of China include the Eocene Nadu Formation (E_{2n}), Baigang Formation (E_{2b}), and the Oligocene Fuping Formation (E_{3f}) and Jianduling Formation (E_{3j}). The exposed stratum on the surface is the Jianduling Formation (E_{3j}), and the Nadu Formation beneath the regional caprock forms a low-pressure system with a pressure coefficient of less than 0.9. In the late Oligocene, the basin began to uplift as a whole, with a stratum denudation thickness greater than 1200 m at the basin margin and greater than 800 m at the basin center [57]. The static time is greater than 23.5 Ma, which is also consistent with the long-term static low-pressure model.

The Songliao Basin experienced folding and atrophy in the Late Cretaceous, undergoing passive uplift and subsidence under compression, followed by a slow cessation of tectonic activity. In the Cenozoic era, it remained in a tectonically inactive static stage for a long time. The eastern Nenjiang Formation (k_{2n}) was denuded, exhibiting low to normal pressure; only the Qijia-Gulong Depression has 130 m of Cenozoic sediment, showing normal to slightly high pressure.

5.3. Example of Passive Pressurization Mode

There exists passive overpressure in the Yichang area of the Middle Yangtze region. This area has experienced multiple episodes of tectonic uplift and subsidence. Large-scale uplift began at the end of the Triassic period (200 Ma), followed by rapid subsidence in the Early Cretaceous and another rapid uplift during the Miocene and Pliocene (10–5 Ma) [58,59]. This has led to the formation of passive overpressure, with an overpressure coefficient reaching 1.4 times [60]. The theoretical maximum uplift height is calculated to be 1100 m (using the depth of 2800 m in the E'yi Ye-2 well), which is consistent with the results obtained by Tang et al. (2011) [61].

Passive overpressure is also present in the Wuwei Depression of the Lower Yangtze region. In 2019, two sets of abnormally high-pressure natural gas-bearing layers were discovered for the first time in the Triassic Zhouchongcun Formation T_{2z} of the Wanwei Ye-1 well, with a maximum formation pressure coefficient of 1.9 [62]. The shallow first gypsum salt layer, which is nearly 200 m thick (1975–2175 m), blocks the escape of formation water and natural gas, with a pressure coefficient of 1.79. The second gypsum salt layer beneath it is 50 m thick (2295–2345 m) and has a pressure coefficient of 1.95 (Figure 7). There has been relatively recent rapid uplift and denudation in this area (compared to the Miocene and Pliocene), resulting in slow release of formation pressure within better or thicker cap rocks. Large-scale vertical movement only occurred in eastern China during the Oligocene, with denudation of the Paleogene in southern Jiangsu reaching 2000–3000 m [63]. Zeng (2005) [64] used paleotemperature parameters to reconstruct the tectonic evolution of the Wuwei Depression in the Lower Yangtze region, indicating large-scale uplift and denudation in the study area, resulting in the widespread absence of Jurassic strata, with denudation reaching up to 2550 m during this period. As seen from the aforementioned examples, the pressure release due to uplift and denudation becomes slower as it approaches the present day. Ideally, it should be controlled within 5 Ma, as in the case of uplift in the Sichuan Basin mentioned earlier. The uplift in this area occurred during the Oligocene (37–23.5 Ma). If it were conventional mudstone, the internal high pressure should have been fully released. However, the presence of two gypsum salt layers in the Wuwei Depression has slowed down this process.

Abnormally high pressures have been observed in the Permian and Triassic reservoirs of the Mahu Sag in the northwest Junggar Basin [65], with a maximum overpressure coefficient reaching 1.9 times, exhibiting similar characteristics. During the Neogene period, the basin experienced intense tilting, resulting in uplift in the north and subsidence in the south. The strong subsidence in front of the Northern Tianshan Mountains caused Neogene sediments to accumulate mainly in this area, while the northern part of the basin was predominantly an uplifted and denuded region [66]. Only a portion of the

Paleogene strata in the Mahu Sag is preserved in the eastern part. As observed from the northwest–southeast profile across the Mahu Sag, the Cenozoic strata gradually thicken towards the southeast. The minimum residual thickness in the Mahu Sag is 200 m, while it can reach up to 4 km in the Fukang Sag [67]. Based on these observations, it can be inferred that the uplift and denudation in the Mahu Sag are closely related to the intense compression and thrusting from the southern Tianshan Mountains during the Neogene period. The large denudation thickness and relatively recent timing (Pliocene or later) are consistent with the passive pressurization model. Using Formula (2) for this model, the theoretical denudation thickness is calculated to be greater than 4 km.

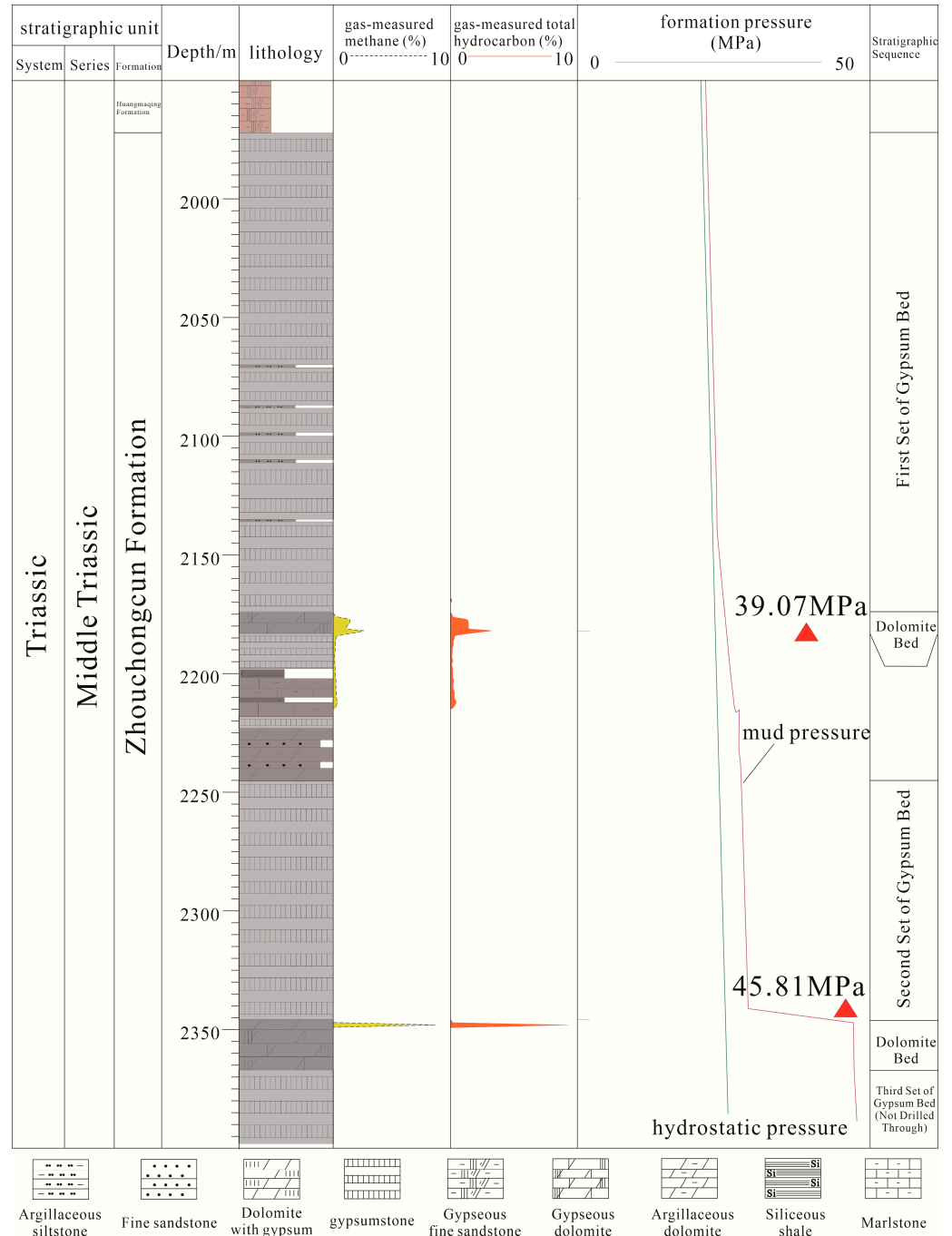


Figure 7. Oil and gas shows in the Triassic Zhouchongcun Formation of well Wanwei Ye 1 in the Wuwei Depression [62]. Methane is generally represented in yellow, while total hydrocarbons are typically shown in red. The triangle symbol denotes the actual measurement points of formation pressure.

5.4. Formation Pressure Model

Refer to Table 4 for more examples. The data in the table are plotted on a semilogarithmic coordinate system of tectonic movement rate v and pressure coefficient c to illustrate their correlation. Positive values represent deposition or subsidence, while negative values represent uplift and erosion. More than 50 famous large basins or regions, both domestically and internationally, were collected. Among them, only 43 basins with both stratigraphic pressure data c and tectonic movement rate v were retained [68–92]. The data were directly plotted without any filtering, as shown in Figure 8.

Table 4. Overpressure and structural conditions of each basin.

No.	Basin	Pressure Coefficient	Depth of the Top Surface of Abnormal Pressure (m)	Uplift Sediment Thickness (m)	Start Time (Ma)	Lifting and Lowering Rate * (m/Ma)	Literature Source
1	Junggar Basin	1.9	2500	−4000	5.2	−769	Zhang et al., 2022 [65]
2	Qiongdongnan Basin	2.0	2900	2000	2.0	1000	Hao et al., 2015 [26]
3	Qaidam Basin	2.0	2000	1500	5.2	288	Zhang et al., 2016 [52]
4	Jizhong Depression	1.37	3300	2000	3.5	85	Hou et al., 2012 [51]
5	Tarim Basin	2.2	4600	1800	5.2	346	Wang, 2016 [50]
6	Alberta Basin	1.0				0	Wang et al., 2016 [90]
7	Baise Basin	0.9	2000	−800	23.5	−34	Zou et al., 2003 [57]
8	Songliao Basin	1.0	3000	130	83	1.6	Xiang et al., 2006 [41]
9	Lower Yangtze Region	1.90	2000	−3000	37	−83	Yao et al., 1999 [63]
10	Ordos Basin	0.85	3000	600	23.5	25.5	Li et al., 2012 [47]
11	Sichuan Basin	2.2		−3000	5.0	−600	Deng et al., 2009 [39]
12	Bohai Bay Basin	1.6	3200	2100	5.1	411	Zhang, 2018 [35]
13	West Lake Depression	1.5	3900	8500	24	354	Liu, 2023 [68]
14	Huimin Depression	1.78	3000	1500	25	62.5	Huo, 2020 [69]
15	Erlian Basin	1.0	1300	−180	24	−7.5	Xu, 2007 [43]
16	Pearl River Estuary Basin	1.8	3000	3800	Hanjiang Formation	237	Zhang, 2023 [70]
17	Jiyang Depression	1.7	3400	1500	5	300	Gong, 2005 [71]
18	Kuqa Foreland Basin	2.16	4000	1500	3	179.01	Zhang, 2011 [72]
19	Yinggehai Basin	1.9	4500	500	1.5	250	Mao et al., 2022 [73]
20	Liaohe Basin	1.96	3400	800	8	100	Peng et al., 2013 [74]
21	Yine Basin	1.3	2200	1100	Early Cretaceous	18.33	Zhang et al., 2020 [75]
22	Lunpola Basin	1.0	2100	1000	36.4	25.58	Liu, 2020 [76]
23	Yine Basin	1.429	2000		Early Cretaceous	400	Hou et al., 2019 [77]
24	Hailar Basin	0.81	1700	700	Lower Cretaceous	0	Wang et al., 2010 [78]
25	Yitong Basin	1.1	2500	200	Early-Mid Eocene	190	Wang, 2016 [79]
26	Jiuquan Basin	1.84	3700		Lower Cretaceous	470	Zhou et al., 2013 [80]
27	Yitong Basin	1.0	2304	800		100	Cao et al., 2011 [81]
28	Qaidam Basin	2.1	2300		Eocene Series	330	Han et al., 2023 [82]
29	Gulf of Mexico	1.2	5600	500	29	34.5	Zhang, 2023 [83]
30	Irrawaddy Basin	2.20	1500		Eocene	1500	Chen et al., 2014 [84]
31	Junggar Basin	2.46	2710		Jurassic	500	Lu et al., 2022 [85]
32	Sichuan Basin	1.7		2500	Jurassic	−100	Liu, 2020 [86]
33	Sichuan Basin	1.85	2400		Middle Jurassic	−150	Liu et al., 1995 [87]
34	Middle Yangtze Region	1.4	2700	−1100	8	−137	Zhang et al., 2019 [60]
35	West Kunlun Mountains	2.05	4000	−4000	2	−2000	Ma et al., 2022 [88]
36	Biyang Depression	1.15		300	5	60	Zhang et al., 2020 [89]
37	Fort Worth	1.1	1980	50	24	2	Wang et al., 2016 [90]
38	Guizhou	1.0	1200	80	480	0.1	Wang et al., 2016 [90]
39	Sichuan Basin	1.5		−3100	20.9	−148	Xue et al., 2023 [91]
40	Sichuan Basin	1.18		−700	31	−22.6	Xue et al., 2023 [91]
41	Sichuan Basin	1.1		−1600	26	−61	Xue et al., 2023 [91]
42	Illinois	0.99	−3000	250	64	−3.8	Wang et al., 2016 [90]
43	Qinghai-Tibet Region	1.05	3000	−650	24	−27	Wang et al., 2020 [92]

* Positive numbers represent subsidence, while negative numbers represent uplift.

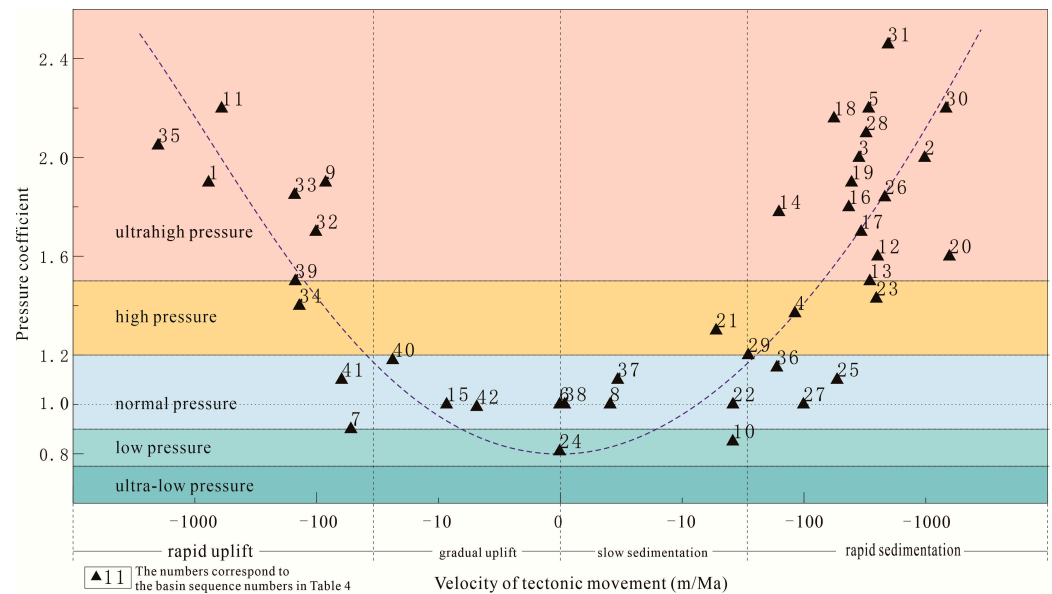


Figure 8. Relationship between tectonic movement velocity and overpressure.

Using quadratic curve fitting (dashed line in the figure), the following formula is obtained:

$$c = 0.13(\log_{10} |v|)^2 + 0.008 \log_{10} |v| \times \sin(v) + 0.95 \quad (4)$$

where v represents the tectonic movement velocity, measured in meters per million years (m/Ma); c is the pressure coefficient; and $\sin(v)$ takes the sin of v . The goodness of fit, R^2 , reaches 0.64, indicating a relatively good fitting effect.

6. Results and Conclusions

Studying the influencing factors of formation pressure with the clue of formation water permeability, the following results are obtained:

- (1) The formation pressure coefficient depends on the permeability of formation water and is positively correlated with the velocity of tectonic movement. The faster the tectonic movement in the Neogene or Quaternary, the more prone to overpressure, while slow tectonic movement in the Cenozoic is dominated by normal or low pressure.
- (2) Compared to pore space, the space vacated by overpressure to normal pressure or the space squeezed is small, less than an order of magnitude observed as abnormally high porosity (5–17%) attributed to undercompaction.
- (3) Physical simulation experiments or numerical simulations of hydrocarbon generation and pressurization are conducted in a completely closed state, accelerating the process of compaction, diagenesis, and hydrocarbon generation faster than the escape rate of formation water, which does not represent real underground geological conditions. Under actual formation conditions, most tectonic activities and hydrocarbon generation processes occur on a time scale that is an order of magnitude larger than the escape rate of formation water. There is no direct correlation between overpressured compartments and the presence of hydrocarbons.

The conclusion is as follows:

- (1) The pressure state of the stratum mainly depends on the mode and intensity of tectonic activity in the late Cenozoic era. Both rapid uplift and rapid subsidence during the late Cenozoic can produce overpressure phenomena, while prolonged slow uplift or neither uplift nor depositional subsidence will result in normal or low pressure.
- (2) There is a positive correlation between the recent tectonic movement's velocity of ascent and descent and the pressure coefficient.

- (3) Four models of stratum pressure are proposed, i.e., active overpressure model of rapid subsidence (Nanpu Model), passive overpressure model of rapid uplift (Sichuan Model), long-term static normal pressure model (Songliao Model), and large uplift with small subsidence low pressure model (Sulige Model). These models can determine the stratum pressure state within a unified theoretical framework.
- (4) A method for calculating the amount of denudation using the characteristics of formation water pressure relief, as well as a method for calculating the maximum height of tectonic uplift, are proposed.
- (5) Other hypotheses for the causes of overpressure, such as undercompaction, tectonic compression, and hydrocarbon generation pressurization, may exist. However, their impact on overpressure is not significant.

This article will help us gain a new perspective on the concept of overpressure formation mechanisms related to sedimentology and petroleum geology.

Author Contributions: Writing—original draft preparation, X.M.; writing—review and editing, S.L.; visualization, X.C.; supervision, X.L. and F.Y.; project administration, Y.Y. and Z.L.; funding acquisition, Y.Y. All authors have read and agreed to the published version of the manuscript.

Funding: This research received no external funding.

Institutional Review Board Statement: Not applicable.

Informed Consent Statement: Not applicable.

Data Availability Statement: No new data were created or analyzed in this study. Data sharing is not applicable to this article.

Acknowledgments: The authors acknowledge anonymous reviewers for their assistance.

Conflicts of Interest: The authors declare that they have no known competing financial interests or personal relationships that could have appeared to influence the work reported in this paper.

References

1. Hunt, J.M. Generation and migration of petroleum from abnormally pressured fluid compartments. *AAPG Bull.* **1990**, *74*, 1–12.
2. Jin, Z.; Xie, F. Distribution features of formation pressure in typical petroliferous basin of China. *J. China Univ. Pet. Ed. Nat. Sci.* **2002**, *26*, 1–6.
3. Xie, X.; Wang, Z. Dynamics of basin fluid and its advances. *Acta Sedimentol. Sin.* **2003**, *21*, 19–23.
4. Hao, F.; Zou, H.; Ni, J.; Zeng, Z.; Wang, M. Evolution of overpressure systems in sedimentary basins and conditions for deep oil/gas accumulation. *J. China Univ. Geosci.* **2002**, *27*, 610–615.
5. Hao, F.; Dong, W. Evolution of fluid flow and petroleum accumulation in overpressured systems in sedimentary basins. *Adv. Earth Sci.* **2001**, *16*, 79–85.
6. Hao, F.; Zou, H.; Jiang, J. Dynamics of petroleum accumulation and its advances. *Earth Sci. Front.* **2000**, *7*, 11–21.
7. Wang, Z.; Li, J. Abnormal high pressure and its relation to hydrocarbon accumulation in Raoyang Sag. *Lithol. Reserv.* **2014**, *26*, 15–19.
8. Du, X.; Zheng, H.; Jiao, X. Abnormal pressure and hydrocarbon accumulation. *Earth Sci. Front.* **1995**, *4*, 137–148.
9. Hunt, J.M. *Petroleum Geology and Geochemistry*; Freeman: San Francisco, CA, USA, 1996; p. 743.
10. Hao, F.; Zhou, H.; Yang, X.; Wang, M. Episodic petroleum accumulation, its driving mechanisms and distinguishing markers. *Chin. J. Geol.* **2003**, *38*, 413–424.
11. Feng, Z.; Zhang, S.; Feng, Z. Discovery of “Enveloping Surface of Oil and Gas Overpressure Migration” in the Songliao Basin and its bearings on hydrocarbon migration and accumulation mechanisms. *Sci. Chin. Earth Sci.* **2011**, *41*, 1872–1883. [[CrossRef](#)]
12. Huang, C.; Ni, X.; Ma, X.; Gao, Y.; Zhang, Z.; Yang, S.; Cui, J.; Zhao, Q. Petroleum and gas enrichment pattern and major controlling factors of stable and high production of tight lacustrine carbonate rock reservoirs: A case study of the Yingxi area in Qaidam Basin. *J. Northwest Univ. Nat. Sci. Ed.* **2017**, *47*, 724–738.
13. Meissner, F.F. Mechanisms and patterns of gas generation storage expulsion-migration and accumulation associated with coal measures Green River and San Juan Basin Rocky mountain region, USA. In Proceedings of the 2nd IFP Exploration Research Conference, Carcans, France, 15–19 June 1987.
14. Luo, X.; Yang, J.; Wang, Z. The overpressuring mechanisms in aquifers and pressure prediction in basins. *Geol. Rev.* **2000**, *46*, 22–31.
15. Wang, X.; Wu, J.; Ran, Y.; Jia, S.; Zhang, N. Influence of non-linear flow on productivity of abnormal high pressure gas reservoir. *Lithol. Reserv.* **2012**, *24*, 125–128.

16. Liu, X.; Xie, X. Review on formation mechanism of the reservoir overpressure fluid system. *Bull. Geol. Sci. Technol.* **2003**, *22*, 55–60.
17. Wan, Z.; Xia, B.; He, J.; Liu, B. Formation mechanism of overpressure and its influence on hydrocarbon accumulation in sedimentary basins. *Nat. Gas Geosci.* **2007**, *18*, 219–222.
18. Wang, Z.; Li, Y.; Zhang, J. Analysis on main formation mechanisms of abnormal fluid pressure in the Upper Triassic, west Sichuan area. *Oil Gas Geol.* **2007**, *28*, 43–50.
19. Li, C. Can uplift result in abnormal high pressure in formation? *Lithol. Reserv.* **2008**, *20*, 124–126.
20. Qu, J.; Wang, Z.; Ren, B.; Bai, Y.; Wang, B. Genetic mechanism analysis and prediction method of abnormal high pressure in Mahu slope area, Junggar Basin. *Lithol. Reserv.* **2014**, *26*, 36–39.
21. Wang, Z.; Hao, C.; Li, J.; Feng, Z.; Huang, C. Distribution and genetic mechanism of overpressure in western Sichuan foreland basin. *Lithol. Reserv.* **2019**, *31*, 36–43.
22. Law, B.E.; Ulmishek, G.F.; Slavin, V.I. *Abnormal Pressures in Hydrocarbon Environments (AAPG Memoir70)*; The American Association of Petroleum Geologists: Tulsa, OK, USA, 1994.
23. Osborne, M.J.; Swarbrick, R.E. Mechanisms for generating overpressure in sedimentary basins: A reevaluation. *AAPG Bull.* **1997**, *81*, 1023–1041.
24. Bethke, C.M. Inverse hydrologic analysis of the distribution and origin of gulf coast-type geopressed zones. *J. Geophys. Res. Solid Earth* **1986**, *91*, 6535–6545. [[CrossRef](#)]
25. Qiu, N.; Liu, Y.; Liu, W.; Jia, J. Quantitative reconstruction of formation paleo-pressure in sedimentary basins and case studies. *Sci. Chin. Earth Sci.* **2020**, *63*, 808–821. [[CrossRef](#)]
26. Hao, F.; Jiang, J.; Zou, H.; Fang, Y.; Zeng, Z. The overpressure differently and levelly retard the organic matter evolution. *Sci. Chin. Earth Sci.* **2004**, *34*, 443–451.
27. Magara, K. *Compaction and Fluid Migration: Practical Petroleum Geology*; Elsevier Scientific Pub. Co.: Amsterdam, The Netherlands, 1978.
28. Neuzil, C.E. Abnormal pressures as hydrodynamic phenomena. *Am. J. Sci.* **1995**, *295*, 742–786. [[CrossRef](#)]
29. Chen, Y.; Jia, G.; Luan, J.; Zhang, M.; Zhu, Q.; Li, W. Study on anomaly model of comprehensive geochemical exploration for oil and gas. *Geol. Explor.* 1992. Available online: <https://kns.cnki.net/kcms2/article/abstract?v=gR09I6yibQ7vQPD6uO0kn8VeehCcv8PhJkSsXpDoNLMuCe-sAeP2SFTNGFeLgAZa2I77i7k3NxiOq6i31eBK7CAnx3DaGQmvKIIXOeDQvjWV0dWlTmj5WYvrsdafVgc&uniplatform=NZKPT&flag=copy> (accessed on 13 June 2024).
30. Supple, S.; Quirke, N. Rapid imbibition of fluids in carbon nanotubes. *Phys. Rev. Lett.* **2003**, *90*, 214501. [[CrossRef](#)]
31. Li, C.; Li, D. Imbibition is not caused by capillary pressure. *Lithol. Reserv.* **2011**, *23*, 114–117.
32. Wu, L. Quantitative relationship between shale NMR transverse relaxation time and pore size distribution and its application. *Pet. Geol. Recovery Effic.* **2024**, *31*, 36–43.
33. Li, G.; Zhao, Z.; Liu, D. Research on Temporal and Spatial Evolution Law of Groundwater Flow Field in Mining Area Under Strong Perturbation Conditions. *Min. Technol.* **2024**, *24*, 136–144.
34. Yu, Z.; Huang, Y. *Principles of Groundwater Hydrology*; Science Press: Beijing, China, 2008; pp. 20–21.
35. Zhang, L.; Xiang, C.; Dong, Y.; Zhang, M.; Lyu, Y.; Zhao, Z.; Long, H.; Chen, S. Abnormal pressure system and its origin in the Nanpu Sag, Bohai Bay Basin. *Oil Gas Geol.* **2018**, *39*, 664–675.
36. Yang, J.; Ji, Y.; Wu, H.; Meng, L. Diagenesis and Porosity Evolution of Deep Reservoirs in the Nanpu Sag: A case study of Sha 1 Member of the Paleogene in No. 3 structural belt. *Acta Sedimentol. Sin.* **2022**, *40*, 203–216.
37. Mckenzie, D.S. Remarks on the development of sedimentary basins. *Earth Planet. Sci. Lett.* **1978**, *40*, 25–32. [[CrossRef](#)]
38. Xia, X.; Zeng, F.; Song, Y. Is tectonic uplifting the genesis of abnormal highpressure? *Pet. Geol. Exp.* **2002**, *24*, 496–500.
39. Deng, B.; Liu, S.; Liu, S.; Li, Z.; Zhao, J. Restoration of exhumation thickness and its significance in Sichuan Basin, China. *J. Chengdu Univ. Technol. Sci. Technol. Ed.* **2009**, *36*, 675–686.
40. Wang, E.; Meng, Q. Mesozoic and Cenozoic tectonic evolution of the Longmenshan fault belt. *Sci. Chin. Earth Sci.* **2008**, *38*, 1221–1233. [[CrossRef](#)]
41. Xiang, C.; Feng, Z.; Wu, H.; Pang, X.; Li, Q. Three abnormal pressure systems developed in the Songliao Basin, northeast China and their genesis. *Acta Geol. Sin.* **2006**, *80*, 1752–1759.
42. Chen, Z.; Liu, G.; Lu, X.; Huang, Z.; Luo, Q.; Ding, X. Quantitative study of inversion degree of inversion structure in Erlian Basin and its influence on oil and gas accumulation. *J. Cent. South Univ.* **2015**, *46*, 4136–4145.
43. Xu, X.; Liu, Z.; Xiao, W.; Hao, Q.; Zhao, X.; Yang, D. Discussion on the genesis mechanism of abnormal low pressure in Erlian Basin. *J. China Univ. Pet. Ed. Nat. Sci.* **2007**, *2*, 13–18.
44. Xue, Z.; Qu, Z.; Cheng, J.; Wang, Y.; Ma, Y.; Xu, Y. Restoration of denudation in Jieryangtu Sag in Erlian Basin and its influence on oil and gas reservoirs. *Geol. J. China Univ.* **2019**, *25*, 714–721.
45. Zhang, W.; He, F.; Yan, X.; Lu, Y.; Cai, L.; An, C. Tectonic superposition and accumulation of natural gas in northern Ordos Basin. *J. China Univ. Min. Technol.* **2022**, *51*, 689–703.
46. Zhao, J.; Liu, C.; Wang, X.; Ma, Y.; Huang, L. Uplifting and evolution characteristics in the Lüliang Mountain and its adjacent area during the Meso-Cenozoic. *Geol. Rev.* **2009**, *55*, 663–672.
47. Li, X.; Feng, S.; Li, J.; Wang, M.; Huang, X.; Wang, K.; Kong, L. Geochemistry of natural gas accumulation in Sulige large gas field in Ordos Basin. *Acta Petrol. Sin.* **2012**, *28*, 836–846.
48. Zeng, L.; Zhou, T.; Lyu, X. Influence of tectonic compression on the abnormal formation pressure in the Kuqa depression. *Geol. Rev.* **2004**, *50*, 471–475.

49. Wang, B.; Qiu, N.; Wang, X.; Zhang, H.; Liu, Y.; Chang, J.; Zhu, C. Identification and calculation of tectonic compression overpressure of Kelasu–Yiqikelike tectonic belt in Kuqa depression. *Acta Pet. Sin.* **2022**, *43*, 1107–1121.
50. Wang, X.; Wei, H.; Shi, W.; Wang, Y. Characteristics of formation pressure and its relationship with hydrocarbon accumulation in the eastern part of kuqa depression. *Bull. Geol. Sci. Technol.* **2016**, *35*, 68–73.
51. Hou, F.; Dong, X.; Wu, L.; Li, X.; Hou, F. Abnormal overpressure and hydrocarbon pooling in Maxi sag, Jizhong depression. *Nat. Gas Geosci.* **2012**, *23*, 707–712.
52. Zhang, J.; Zhang, J.; Yang, Q.; Wu, C.; Cui, Q.; Wang, Y.; Guo, L. The control effect of gypsum-salt rocks on formation and distribution of overpressure: A case of Shizigou area, Qaidam Basin. *Acta Sedimentol. Sin.* **2016**, *34*, 563–570.
53. Hao, F.; Liu, J.; Zou, H.; Li, P. Mechanisms of natural gas accumulation and leakage in the overpressured sequences in the Yinggehai and Qiongdongnan basins, offshore South China Sea. *Earth Sci. Front.* **2015**, *22*, 169–180.
54. Corbet, T.F.; Bethke, C.M. Disequilibrium fluid pressures and groundwater flow in the Western Canada sedimentary basin. *J. Geophys. Res. Solid Earth* **1992**, *97*, 203–7217. [[CrossRef](#)]
55. Bachu, S.; Underschlutz, J.R. Large-scale underpressuring in the Mississippian—Cretaceous succession, southwestern Alberta basin. *AAPG Bull.* **1995**, *79*, 989–1004.
56. Allan, J.; Creaney, S. Oil families of the western Canada basin. *Bull. Can. Pet. Geol.* **1991**, *39*, 107–122.
57. Zou, H.; Hao, F.; Cai, X. Summarization of subnormal pressures and accumulation mechanisms of subnormally pressured petroleum reservoirs. *Bull. Geol. Sci. Technol.* **2003**, *22*, 45–50.
58. Yu, W.; Shen, C.; Yang, C. Fission track constraints on Mesozoic tectonic-thermal evolution in the Zigui Basin. *Earth Sci. Front.* **2017**, *24*, 116–126.
59. Li, T.; He, S.; He, Z.; Wo, Y.; Zhou, Y.; Wang, F.; Yang, X. Tectonic uplift and thermal history reconstruction of Dangyang syncline since Mesozoic in the Middle Yangtze region. *Acta Pet. Sin.* **2012**, *33*, 213–224.
60. Zhang, J.; Xu, H.; Zhou, Z.; Ren, P.; Guo, J.; Wang, Q. Geological characteristics of shale gas accumulation in Yichang area, western Hubei. *Acta Pet. Sin.* **2019**, *40*, 887–899.
61. Tang, J.; Mei, L.; Zhou, X.; Li, Q. Control of differential tectonic deformation of Yangtze landmasses on hydrocarbon formation evolution in Marine strata. *Nat. Gas Ind.* **2011**, *31*, 36–41.
62. Li, J.; Zhang, C.; Huang, Z.; Fang, C.; Wu, T.; Shao, W.; Zhou, D.; Teng, L.; Wang, Y.; Huang, N. Discovery of overpressure gas reservoirs in the complex structural area of the Lower Yangtze and its key elements of hydrocarbon enrichment. *Geol. Bull. China* **2021**, *40*, 577–585.
63. Yao, B.; Lu, H.; Guo, N. The multi stage structure frame of Lower Yangtze basin evolution and its significance in petroleum geology. *Pet. Explor. Dev.* **1999**, *26*, 10–13.
64. Zeng, P. *The Application of the Thermometric Indicators to the Study of Thermal Evolution in the Lower-Yangtze Region*; China University of Geosciences: Beijing, China, 2005.
65. Zhang, H.; Cheng, L.; Fan, H.; Wang, G.; Mao, R.; Mou, L.; Wu, W.; Xie, X. Formation overpressure and its influence on physical properties in Mahu sag, Junggar Basin. *Adv. Geophys.* **2022**, *37*, 1223–1227.
66. Wang, X.; Song, Y.; Zheng, M.; Guo, X.; Wu, H.; Ren, H.; Wang, T.; Chang, Q.; He, W.; Wang, X.; et al. Tectonic evolution of and hydrocarbon accumulation in the western Junggar Basin. *Earth Sci. Front.* **2022**, *29*, 188–205.
67. He, W.; Fei, L.; Ablimiti, Y.; Yang, H.; Lan, W.; Ding, J.; Bao, H.; Guo, W. Accumulation conditions of deep hydrocarbon and exploration potential analysis in Junggar Basin, NW China. *Earth Sci. Front.* **2019**, *26*, 189–201.
68. Liu, J.; Zhang, G.; Liu, Y. Origin mechanism of abnormal high-pressure compartment in A sub-sag of Xihu sag and its controlling effect on reservoir formation. *China Offshore Oil Gas* **2023**, *35*, 25–33.
69. Huo, Z.; He, S.; Wang, Y.; Guo, X.; Zhu, G.; Zhao, W. Distribution and causes of present-day overpressure of Shahejie Formation in Linnan Subsag, Huimin Sag, Bohai Bay Basin. *Pet. Geol. Exp.* **2020**, *42*, 938–945.
70. Zhang, L.; Zhang, X.; Peng, G.; Liu, B.; Shi, Z. Overpressure simulation and reservoir formation of Baiyun Depression. *J. Xi'an Shiyou Univ. Nat. Sci. Ed.* **2023**, *38*, 30–37.
71. Gong, X.; Jin, Z.; Zeng, J.; Qiu, N. Reservoiring characteristics and main controlling factors for deep hydrocarbon accumulations in Bonan Sag in Jiyang Depression. *Oil Gas Geol.* **2005**, *26*, 473–479.
72. Zhang, F. *Hydrodynamic Characteristics, Evolution and Its Role in Hydrocarbon Accumulation in Kuqa Foreland Basin*; Northwestern University: Xi'an, China, 2012.
73. Mao, Q.; Fan, C.; Luo, J.; Cao, J.; You, L.; Fu, Y.; Li, S.; Shi, X.; Wu, S. Differences in Sedimentary and Diagenetic Evolution of Meso-Deep Sandstone Reservoirs under the Background of Hypoxia: A Case Study of the Middle Miocene Huangliu Formation in the Yinggehai Basin, South China Sea. *J. Palaeogeogr.* **2022**, *24*, 344–360.
74. Peng, B.; Zou, H.; Teng, C.; Hao, F. Development and Evolution of Hyperbaric Pressure in Damintun Depression and Dynamic Mechanism of Oil and Gas Migration and Accumulation. *J. China Univ. Pet. Ed. Nat. Sci.* **2013**, *37*, 10–16.
75. Zhang, H.; Li, J.; Wang, X.; Shi, D.; Chen, Q.; Fan, X.; Si, M.; Zhao, Q. Formation and Evolution of Yingge Basin and Prospects for Oil and Gas Exploration. *Pet. Geol. Exp.* **2020**, *42*, 780–789.
76. Liu, Y. *Dynamics of Hydrocarbon Accumulation in Lunlu La Basin, Tibet*; China University of Geosciences: Wuhan, China, 2020.
77. Hou, Y.; Fan, T.; Wang, H.; Shi, D.; Chen, Q.; Yang, R. Characteristics and Formation Mechanism of High-quality Deep Reservoirs in Guazihu Sag, Yingge Basin. *Acta Sedimentol. Sin.* **2019**, *37*, 758–767.
78. Wang, X. Prediction and Calculation of Three Formation Pressures in the Hailar Area. *Drill. Eng.* **2010**, *37*, 13–18.

79. Wang, W. Analysis of Stratigraphic Pressure Evolution in the Moriging Fault Depression by Basin Simulation Method. *Bull. Geol. Sci. Technol.* **2016**, *35*, 103–109.
80. Zhou, Y.; Liu, G.; Zhong, J.; Liu, Q.; Yu, H. Genesis and Simulation of the Lower Cretaceous Abnormal High Pressure in Ying'er Sag, Jiuquan Basin. *J. Cent. South Univ.* **2013**, *44*, 2402–2409.
81. Cao, Q.; Ye, J. Stratigraphic Pressure Evolution and Hydrocarbon Migration Simulation in the Moriging Fault Depression, Yitong Basin. *Pet. Explor. Dev.* **2011**, *38*, 174–181.
82. Han, T.; Liu, C.; Tian, J.; Yang, T.; Feng, D.; Li, G. Formation Mechanism of Hyperbaric Pressure in Youquanzi Oilfield, Western Qaidam Basin. *Spec. Oil Gas Reserv.* **2024**, *31*, 37–46.
83. Zhang, X. *Geological Characteristics, Formation Conditions and Accumulation Model of Deep Oil and Gas Reservoirs in the Gulf of Mexico Basin*; China University of Petroleum: Beijing, China, 2023.
84. Chen, H.; Li, Z.; Guo, M. Overpressure and Hydrocarbon Accumulation in Block D of Myanmar. *Nat. Gas Tec. Eco.* **2014**, *8*, 78.
85. Lu, X.; Zhao, M.; Zhang, F.; Gui, L.; Liu, G.; Zhuo, Q.; Chen, Z. Development Characteristics, Genesis and Accumulation Control of Overpressure in the Frontal Thrust Belt of Southern Margin of Junggar Basin. *Pet. Explor. Dev.* **2022**, *49*, 859–870. [[CrossRef](#)]
86. Liu, W. *Research on Stratigraphic Pressure of Sinian-Paleozoic in the Western-Central Sichuan Basin*; China University of Petroleum: Beijing, China, 2020.
87. Liu, B.; Bei, D.; Wang, J. Formation and Evolution of Abnormal High Pressure in Northwestern Sichuan Basin. *Nat. Gas Ind.* **1995**, *15*, 8–12.
88. Ma, H.; Liu, Y.; Qiu, N.; Chen, X.; Wang, X.; Chen, C. Relationship between overpressure and hydrocarbon accumulation in the southern piedmont of West Kunlun Mountains. *Nat. Gas Geosci.* **2022**, *33*, 2049–2061.
89. Zhang, X.; Chen, H.; Long, Z.; Liu, Q. Hydrocarbon migration and accumulation process of Hetaoyuan Formation in the northern gentle slope zone of Biyang Depression. *Bull. Geol. Sci. Technol.* **2020**, *39*, 140–149.
90. Wang, R.; Ding, W.; Gong, D.; Leng, J.; Wang, X.; Yin, S.; Sun, Y. Gas preservation conditions of marine shale in northern Guizhou area: A case study of the Lower Cambrian Niutitang Formation in the Cen'gong block, Guizhou Province. *Oil Gas Geol.* **2016**, *37*, 45–55.
91. Xue, G.; Xiong, W.; Zhang, P. Genesis analysis and effective development of normal pressure shale gas reservoir: A case of Wufeng-Longmaxi shale gas reservoir in Wulong area, Southeast Sichuan Basin. *Reserv. Eval. Dev.* **2023**, *13*, 668–675.
92. Wang, R.; Wu, X.; Xia, X.; Li, Y.; Cao, J. Application of basin simulation technology on the assessment of hydrocarbon resources potential of the Lunpola Basin in Tibet. *J. Geomech.* **2020**, *26*, 84–95.

Disclaimer/Publisher's Note: The statements, opinions and data contained in all publications are solely those of the individual author(s) and contributor(s) and not of MDPI and/or the editor(s). MDPI and/or the editor(s) disclaim responsibility for any injury to people or property resulting from any ideas, methods, instructions or products referred to in the content.